CHINESE OPTICS LETTERS

Vol. 21, No. 10 | October 2023

High energy efficiency soliton microcomb generation in high coupling strength, large mode volume, and ultra-high-Q micro-cavity

Wenwen Cui (崔雯雯), Zheng Yi (易 正), Xinyu Ma (马新宇), Yong Geng (耿 勇)*, Heng Zhou (周 恒), and Kun Qiu (邱 昆)

Key Laboratory of Optical Fiber Sensing and Communication Networks, School of Information and Communication Engineering, University of Electronic Science and Technology of China, Chengdu 611731, China

*Corresponding author: gengyong@uestc.edu.cn

Received April 19, 2023 | Accepted June 9, 2023 | Posted Online October 10, 2023

The nonlinear physics dynamics of temporal dissipative solitons in a microcavity hinder them from attaining high power from pump lasers with a typical nonlinear energy conversion efficiency of less than 1%. Here, we experimentally demonstrate a straightforward method for improving the output power of soliton combs using a silica microrod cavity with high coupling strength, large mode volume, and high-Q factor, resulting in a low-repetition-rate dissipative soliton (~21 GHz) with an energy conversion efficiency exceeding 20%. Furthermore, by generating an ~105 GHz 5 × FSR (free spectral range) soliton crystal comb in the microcavity, the energy conversion efficiency can be further increased up to 56%.

Keywords: optical microcavity; nonlinear optics; temporal soliton.

DOI: 10.3788/COL202321.101902

1. Introduction

Compact optical frequency combs that are based on microcavities have attracted attention due to their potential applications in coherent communications, frequency metrology, photonic frequency synthesis, and quantum optics[1–4]. The Kerr combs emerge as a result of cascaded four-wave mixing (FWM) in optical microcavities. Such nonlinear FWM-based Kerr combs can transform into a low-noise state when the pump is tuned into the red-detuning regime of the pumped resonance mode to obtain dissipative Kerr solitons (DKSs). The DKSs circulating in the optical microcavities rely on the double balance between the Kerr nonlinear phase shift and the cavity dispersion, as well as between the Kerr parametric gain and the cavity decay[5,6].

However, the energy conversion efficiency (ECE) of DKS microcombs is quite low, which casts doubt over their practical utilization[7–9]. There are many reasons for such low ECE. First, when the Kerr comb is operating at a soliton state, the pump field is fixed at the red-detuning regime of the cavity mode, which is noticeably away from the resonance center. That is to say, most of the pump power is directly transferred to the output port of the bus waveguide and does not circulate in the microcavity to support DKS generation. Second, in the time domain, the DKS has an ultra-short optical pulse that is much shorter than the cavity roundtrip time, meaning that the overlap between the DKS pulse and the continuous-wave (CW) pump field is quite small. This hinders the nonlinear interaction and the energy transfer between the pump field and the DKS pulse. Especially for low-repetition-rate DKS combs, the large size of the microcavity has a much larger roundtrip time, which causes much lower ECE. Third, for the microcavity design, there is a trade-off between the Q-factor and the coupling coefficient. The coupling gap between the bus waveguide and the resonator is usually maximized to guarantee that the microcavity has a high Q-factor, which has to sacrifice the energy coupling efficiency from the bus waveguide into microcavity. Such a design rule will block the flow of pump energy into the microcavity, resulting in low ECE. An overview of the ECE of the DKS combs generated in different material microcavities is summarized in Fig. 1. Here, the ECE is characterized by the power difference between the CW pump and the DKS comb spectrum envelope. The ECE is quite low in all different material platforms if there are no energy-enhancing strategies being applied in the experiments. The typical power difference is larger than 20 dB, as shown in Fig. 1. To date, several schemes have been proposed to address the above challenges, such as inducing an extra phase shift to the pump mode[10], using a coupled fiber ring[11], generating a dark soliton[12], forming soliton crystal combs[13], and using a synchronously pulsed pumping technique[14]. Nevertheless, these prior schemes either require complex device structures or sacrifice the performance of the Kerr combs.

In this work, we numerically and experimentally investigate the ECE of DKS combs. First, based on analytical formulas, we shed light on the characterization of the ECE of the DKS

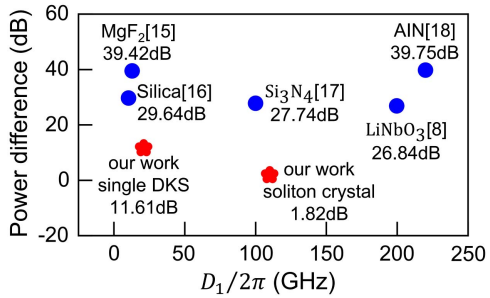

Fig. 1. Overview of the nonlinear energy conversion efficiency of the DKS combs generated in the different nonlinear material platforms. The references for the comparison include MgF_2[15], silica[16], Si_3N_4[17], $LiNbO_3$[8], and AlN[18].

and find that the ECE is dominated by the input pump power, the bus-resonator coupling coefficient, and the nonlinear coefficient. Then, we conduct numerical simulations based on the Lugiato–Lefever equation (LLE) to verify our analytical results. Finally, we fabricate a whispering-gallery-mode (WGM) SiO_2 microrod cavity with a high-Q factor and a large mode volume. Using such a WGM microrod cavity, we experimentally demonstrate a straightforward method for improving the output power of the DKS comb by simply adjusting the bus-resonator coupling coefficient. The ECE of the DKS comb with a 21 GHz repetition rate is achieved at as high as 20%. Furthermore, by generating an ~105 GHz $5\times$ FSR (free spectral range) soliton crystal comb, the ECE is further increased up to 56%.

2. Simulation Results

In an optical microcavity, the nonlinear energy conversion efficiency of the DKS microcomb can be expressed as[19]

$$\eta=\frac{P_s}{P_{\rm in}}=\frac{\theta}{\alpha_i+\theta}\sqrt{\frac{\theta|\beta_2|}{\gamma P_{\rm in}}}\cdot D_1, \tag{1}$$

where $P_{\rm in}$ denotes the incident pump power and P_s denotes the generated soliton power. θ is the coupling rate of the microcavity, and $\alpha=(\alpha_i+\theta)/2$ and α_i denote the total and intrinsic cavity loss, respectively. β_2 denotes the group-velocity dispersion (GVD), γ is the nonlinear coefficient, and D_1 is the free spectral range (FSR) of the microcavity.

It is seen from Eq. (1) that the ECE of the DKS comb in the microcavity is related to the input pump power, the bus-resonator coupling coefficient, and the nonlinear coefficient. To achieve higher ECE, we should resort to using the highest possible Q-factor microcavity (smaller intrinsic loss) with strong coupling strength between the bus and resonator and using the lowest possible incident laser power.

Moreover, to further verify the above findings, we carry out numerical simulations of DKS comb generation in a high-Q WGM microcavity with parameters similar to SiO_2 microcavity used in the experiment. The simulations are based on the Lugiato–Lefever equation and are numerically integrated with the split-step Fourier method[20].

Initially, we study the impact of the nonlinear coefficient (γ) on the ECE. In the simulations, we set the input pump power as 10 mW and a microcavity with critical coupling (both loss α and coupling coefficient θ are 0.000025, corresponding to $Q=6\times10^9$). Following Eq. (1), the DKS comb power is inversely proportional to the nonlinear coefficient γ of the microcavity. As shown in Fig. 2(a), our simulation results confirm such a conclusion. It is seen that the ECE decreases from 4.5% to 3% when the nonlinear coefficient increases from 0.0006 to 0.0018. Subsequently, we vary the coupling strength of the microcavity in the simulation to study the dependence of the bus-resonator coupling coefficient on the ECE. Importantly, in the simulation, we leave the other parameters of the microcavity constant. Figure 2(b) shows that the ECE can be dramatically enhanced from 0.4% to 12.5% by increasing the coupling strength. We attribute such positive results to the larger coupling strength results in the higher pump energy flowing into the microcavity, which then will enhance the nonlinear interaction. Following Eq. (1), we also numerically simulate the variation trends of the ECE with different input pump powers. In this simulation, both the cavity loss and the coupling coefficient are equal to 0.00025, corresponding to critical coupling. The nonlinear coefficient is 0.0015, and the free spectral range is 21 GHz. As illustrated in Fig. 2(c), an increase in input pump power from 2 mW to 10 mW causes the conversion efficiency to decrease from 17.3% to 10.6%.

Thus, to increase the ECE of the DKS comb, we should optimize the parameters of a microcavity. We can reduce the nonlinear coefficient γ or increase the coupling coefficient θ. However, we note that, since these two parameters are closely related to the nonlinear interaction process in the microcavity and the intensity buildup in a microcavity is proportional to Q/V[21], operating with low nonlinear coefficient γ (i.e., a large cavity volume V) and large coupling coefficient θ requires microcavities that have a large Q-factor. Otherwise, such power-enhancing strategies will sacrifice the optical parametric

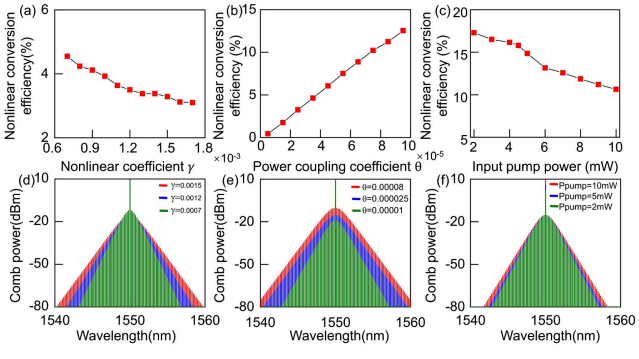

Fig. 2. Nonlinear energy conversion efficiency versus (a) the nonlinear coefficient γ and (b) the power coupling coefficient θ. (c) The input pump power for a silica WGM microcavity with FSR = 21 GHz, $\beta=-150\times10^{-27}$ s^2/m, and $\alpha_i=0.000025$. (d)–(f) Optical spectra for different cavity parameters.

oscillation (OPO) threshold power[22]. So, at the microcavity design stage, there should be a reasonable trade-off between P_{th} and the nonlinear coefficient or the coupling coefficient. Otherwise, a high OPO threshold power will result in a large input pump power and reduce the ECE.

For the nonlinear coefficient, P_{th} is linearly inversely proportional to the nonlinear coefficient γ. Reducing the nonlinear coefficient will cause a higher OPO threshold power in P_{th}. For example, if we set the maximum pump power as 10 mW, the nonlinear coefficient can be minimized to 2.3×10^{-7} to ensure enough pump energy for the OPO operation. On the other hand, the coupling coefficient θ and Q-factor are not independent since the parameter θ matters for the total loss of the microcavity. Thus, we will further discuss in more detail what happens when changing the coupling coefficient θ. The evolution of the ECE of the DKS comb with the sweeping θ and corresponding microcavity per round trip loss α is recorded as shown in Fig. 3. The solid red line denotes the critical coupling state of the microcavity. DKSs generated in the over coupling region can obtain a higher energy conversion efficiency than those generated under the critical coupling regions, as the microcavity with the over coupling state has a larger coupling strength. However, over coupling state will cause a lower quality factor. The quality factors for $Q = 10^9, 5 \times 10^8$, and 2×10^8 are also marked in Fig. 3 using solid lines with different colors. We can see that the extra costs to gain more energy for the DKS comb are low. Such extra coupling loss can be easily compensated by reducing the intrinsic loss of microcavity during the fabrication process. Meanwhile, the OPO threshold of $P_{th} =$ 2 mW is marked with a solid yellow line in Fig. 3, showing that the OPO threshold can be maintained in low-level conditions at a strong coupling state. That is to say that the microcavity with the ultra-high Q can offer more redundancy for improving the coupling strength. Thus, a high-Q microcavity can have both low OPO threshold and large coupling coefficient, which is best suited for high energy efficiency soliton microcomb generation.

3. Experiment Results

To confirm the above theoretical prediction, a high energy efficiency DKS comb generated in a microcavity was experimentally

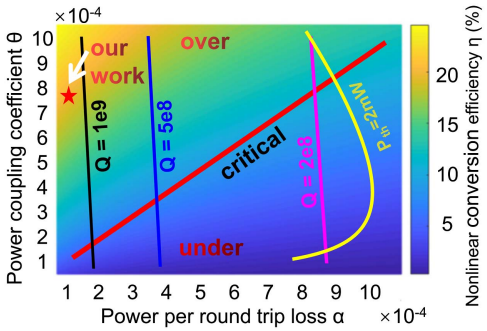

Fig. 3. Evolution of energy conversion efficiency of the DKS comb with the sweeping θ and the corresponding microcavity per round trip loss α.

studied. The challenge in experimentally realizing a high ECE DKS comb is how to fabricate a microcavity with high Q, low nonlinear coefficient, and high coupling strength. First, as we all know, the nonlinear coefficient is determined by both the nonlinear refractive index of the material and the mode area of the microcavity. To obtain a low nonlinear coefficient, the nonlinear refractive index of the material used to fabricate the microcavity should be as small as possible. Meanwhile, the mode area of the microcavity should be as large as possible.

Table 1 summarizes the different nonlinear material platforms for Kerr frequency comb generation. The silica platform has the lowest nonlinear refractive index among all the materials. Another key advantage offered by the silica platform is that the microrod resonator fabricated using this kind of material can achieve the largest mode area as compared with other material platforms. Such a large mode area can further reduce the propagation loss of the optical field caused by resonator surface roughness and thereby boost its Q factor to larger than 1 billion. As discussed above, such ultra-high-Q microcavities can suffer from larger coupling strength and provide more possibility for enhancing the ECE of the DKS combs. Compared with having other DKS comb platforms, the microrod resonator can enable both a low nonlinear coefficient and an ultra-high-Q factor, providing an ideal solution for generating high energy efficiency DKS combs. Moreover, the coupling rate of the WGM resonator can be easily controlled by setting the gap between the fused microrod resonator and a tapered fiber.

Next, we investigate the ECE of the microrod resonator to illustrate the advantage of simultaneously combining a low nonlinear coefficient, an ultra-high-Q factor, and a high bus-resonator coupling strength in this silica resonator platform. The WGM cavity used in our experiment is fabricated by CO_2 laser beam machining on a rotating silica rod[32]. The diameter of the fabricated microrod cavity is about 3 mm, corresponding to an FSR of about 22 GHz. The photograph of the microcavity is shown in Fig. 4(a). Note that the profile of the side wall plays a key role in deciding the mode area and distribution of the resonance modes. So, in the fabricating process, we adjust the distance between the two cutting processes to optimize the profile of the WGM cavity side wall to match our experimental demands. The photograph of the microcavity side wall used in our experiment is also shown in Fig. 4(b). The incident light is coupled into the WGM cavity via a tapered optical fiber. The Q factor and coupling rate are controlled by adjusting the spatial gap between the microrod cavity and the tapered optical fiber. Figure 4(c) shows the mode spectrum of the WGM cavity with a weak coupling strength, and the corresponding Q factor is about 1.87×10^9.

The experimental setup for DKS comb generation is shown in Fig. 5. The auxiliary laser heating (ALH) method is adopted to overcome the thermal instability of the micro-cavity during soliton generation, and details of the ALH method can be found in the previous literature[6]. Of note, in our experiment, the pump and auxiliary laser are derived from the same laser module, and their frequencies and powers are individually adjusted using

Table 1. Performances of the Various Nonlinear Materials for Microcomb Generation at $\lambda \approx 1.55$ μm.

Material	Refractive Index n	Nonlinear Refractive Index n_2 (m^2 W^{-1})	Mode Area A_{eff} (μm^2)	Nonlinear Coefficient γ (m^{-1} W^{-1})	$D_1/2\pi$ (GHz)	Q
Silica microresonator[23]	1.45	2.2×10^{-20}	~240	3.7159×10^{-4}	11.4	2.0×10^9
Silica (wedge disk)[24]	1.45	3×10^{-20}	~60	0.002	9.3	6.7×10^8
Silica (microtoroid)[25]	1.45	3×10^{-20}	~10	0.0122	1 THz	1.2×10^8
Si_3N_4[26]	2.0	2.5×10^{-19}	~1.5	0.6756	200	3.7×10^7
$LiNbO_3$[8]	2.21	1.8×10^{-19}	~1	0.7297	199.7	2.2×10^6
AlGaAs[27]	3.3	2.6×10^{-17}	~0.28	376.4120	1 THz	1.5×10^6
Hydex[28]	1.7	1.15×10^{-19}	~2	0.1331	200	1.0×10^6
Si[29]	3.47	5×10^{-18}	~2	10.1314	127	5.9×10^5
GaP[30]	3.05	7.8×10^{-19}	~0.15	21.0791	500	3×10^5
AlN[31]	2.12	2.3×10^{-19}	~1	0.9323	NA	9.3×10^5

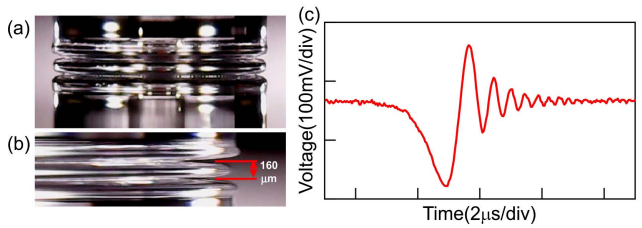

Fig. 4. (a) Picture of the cavity. (b) Picture of the cavity. (c) Q-factor measurement of the SiO_2 microresonator in the time domain.

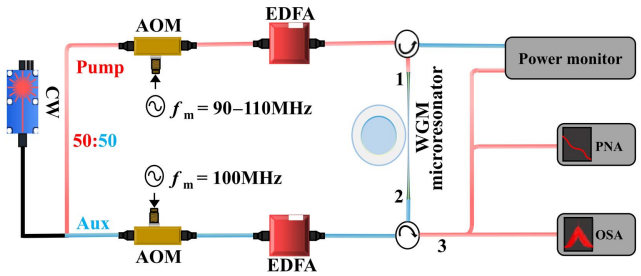

Fig. 5. Experimental setup for soliton microcombs generation using the ALH method.

separate acoustic optical modulators (AOMs) and erbium-doped optical fiber amplifiers (EDFAs). The purpose of using the same laser module for the auxiliary and pump laser is to enhance their mutual frequency stability and to accurately access the shrunken soliton existence range when the pump power becomes low[26], which is crucially important for probing the limit of η at small P_{in}. Specifically, as the pump and auxiliary lasers are from the same laser device and their mutual frequency interval is fixed, the red-detuned pump laser has the same detuning stability as the blue-detuned auxiliary laser, which, by inducing sufficiently strong self-thermal locking, can be very high. It is estimated that, even at the red-detuning regime, the pump laser tuning resolution (as well as the stability of δ) can be as small as 10 kHz, satisfying well the requirement for soliton generation using low pump power and accessing high energy conversion efficiency. For DKS comb generation, the wavelength of the CW laser is centered at 1550 nm. The pump and auxiliary laser fields are boosted to 50 mW and 100 mW, respectively, using two independent EDFAs. These two laser fields are injected into a microrod resonator via a tapered fiber from the counter-propagating direction. Then, the auxiliary laser field is tuned into one cavity mode (centered at 1550 nm) and remained in the blue detuning range at first by adjusting the wavelength of the CW laser. Subsequently, the pump laser field is tuned into the cavity mode from the blue detuning range by controlling the AOM driver frequency. When the pump laser enters the red detuning range, we can access a single DKS comb state adiabatically.

Now, we consider varying the gap between our microrod resonator and the tapered fiber to experimentally investigate the dependence of the ECE on the coupling strength. To study the ECE as a function of the coupling coefficient, this parameter must be measured and tuned in a controlled way. In our experiment, the coupling coefficient is varied by changing the gap distance between our microrod resonator and a tapered fiber. This gap is controlled through a piezo motor and the step size is about 30 nm. In the measurement duration, the coupling state is probed by recording the transmission spectrum of the cavity. For different gap values, the pump laser power remains constant and is set at 5 dBm. Then we measured the transmission of the cavity at different gap values from the over-coupling to the under-coupling state and witnessed an increase in the cavity-loaded Q from about 1.3×10^9 to 4.0×10^9, as shown in

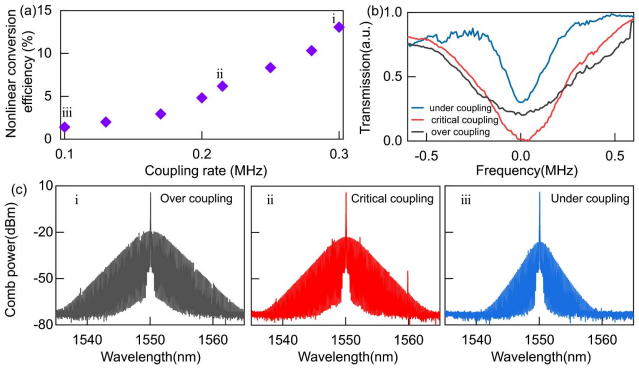

Fig. 6. (a) Nonlinear conversion efficiency versus the input power coupling coefficient. (b) The measured cavity transmission at different coupling rates. (c) The measured optical spectra with different coupling rates.

Fig. 6(b). Figure 6(c) gives the corresponding optical spectra of a single DKS comb. Importantly, it is seen that decreasing the resonator-fiber gap from over coupling to under coupling (i.e., decreasing the coupling coefficient θ), the generated average comb power decreases by more than 7 dB (±3 nm around the pump), and the width of the comb spectral envelop shrinks by 1.4 times. Figure 6(a) shows more detailed measurement results about the ECE with different coupling strengths. The ECE increases from 1.4% to 13% as the input coupling efficiency increases from 0.1 MHz to 0.3 MHz. The results in Fig. 6(a) unambiguously confirm that a larger coupling from a cavity to a bus resonator (and vice-versa) can help to increase the output power of DKS combs.

On the other hand, since the input pump power plays another critical role that impacts the ECE of the DKS comb as discussed above, we next optimize the input pump power to further enhance the conversion efficiency with the over coupling state. In the experiment, we keep the bus-resonator at an over-coupling state using the piezo motor and vary the input pump power by controlling the EDFA output value. Figure 7(a) summarizes the nonlinear conversion efficiency of the DKS comb with different input pump powers. The conversion efficiency increases from 6.7% to 20% as the input pump power P_{in} decreases from 10.5 dBm to 1.67 dBm, approximately consistent with the $P_{\mathrm{in}}^{-0.5}$ trend described in Eq. (1). Figure 7(b) illustrates the generated soliton microcomb optical spectra when the input pump power equals 1.67 dBm. The difference between the DKS

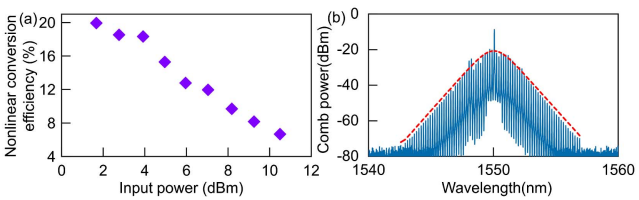

Fig. 7. (a) Nonlinear conversion efficiency in the microcavity with a large coupling strength versus the input power P_{in}. (b) The measured optical spectrum with $P_{\mathrm{in}} = 1.67$ dBm.

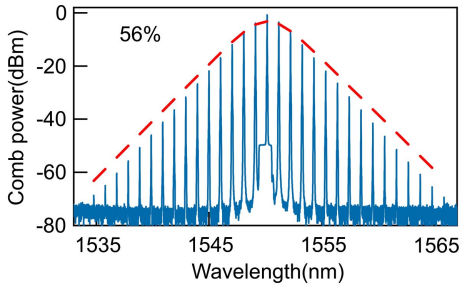

Fig. 8. Measured optical spectrum of the soliton crystal comb characterized with high energy conversion efficiency.

spectrum envelope and the pump comb line is just about 11 dB thanks to the high nonlinear energy conversion efficiency.

In addition to a low nonlinear coefficient, an ultra-high-Q factor, and a high bus-resonator coupling strength, generating soliton crystal combs by maintaining multiple solitons in the microcavity can also significantly enhance nonlinear energy conversion efficiency. Figure 8 shows the optical spectrum of the 5 × FSR soliton crystal comb corresponding to a repetition rate of 110 GHz. As calculated from the comb spectrum, the nonlinear conversion efficiency is up to 56%.

4. Conclusion

In summary, we have demonstrated experimentally that the microcavity characterizing the advantage of simultaneously combining a low nonlinear coefficient, an ultra-high Q-factor, and a high bus-resonator coupling strength can obtain a high nonlinear conversion efficiency for DKS combs. Using a high-Q silica microrod resonator, we achieve a low-repetition-rate dissipative soliton (~21 GHz) with an energy conversion efficiency exceeding 20%. Furthermore, by generating a 5 × FSR (~105 GHz) soliton crystal comb in the microcavity, the energy conversion efficiency can be further increased up to 56%. The results of this work provide a straightforward, low-complexity, highly robust solution for improving the output power of soliton combs.

Acknowledgement

This work was supported by the National Key Research and Development Program of China (Nos. 2019YFB2203103 and 2021YFB-2800602), the National Natural Science Foundation of China (NSFC) (Nos. 62001086 and 61705033), the Sichuan Science and Technology Program (No. 2021YJ0095), and the Fundamental Research Funds for the Central Universities (No. 2021J003).

References

1. Y. Geng, H. Zhou, X. J. Han, W. Cui, Q. Zhang, B. Liu, G. Deng, Q. Zhou, and K. Qiu, "Coherent optical communications using coherence-cloned Kerr soliton microcombs," Nat. Commun. **13**, 1070 (2022).

2. M.-G. Suh, Q.-F. Yang, K. Y. Yang, X. Yi, and K. J. Vahala, "Microresonator soliton dual-comb spectroscopy," Science **354**, 600 (2016).
3. W. Liang, D. Eliyahu, V. S. Ilchenko, A. A. Savchenkov, A. B. Matsko, D. Seidel, and L. Maleki, "High spectral purity Kerr frequency comb radio frequency photonic oscillator," Nat. Commun. **6**, 7957 (2015).
4. C. Reimer, M. Kues, P. Roztocki, B. Wetzel, F. Grazioso, B. E. Little, S. T. Chu, T. Johnston, Y. Bromberg, L. Caspani, D. J. Moss, and R. Morandotti, "Generation of multiphoton entangled quantum states by means of integrated frequency combs," Science **351**, 1176 (2016).
5. T. Herr, V. Brasch, J. D. Jost, C. Y. Wang, N. M. Kondratiev, M. L. Gorodetsky, and T. J. Kippenberg, "Temporal solitons in optical microresonators," Nat. Photonics **8**, 145 (2014).
6. H. Zhou, Y. Geng, W. Cui, S.-W. Huang, Q. Zhou, K. Qiu, and C. W. Wong, "Soliton bursts and deterministic dissipative Kerr soliton generation in auxiliary-assisted microcavities," Light Sci. Appl. **8**, 50 (2019).
7. Q. Wen, W. Cui, Y. Geng, H. Zhou, and K. Qiu, "Precise control of micro-rod resonator free spectral range via iterative laser annealing," Chin. Opt. Lett. **19**, 071903 (2021).
8. Y. He, Q.-F. Yang, J. Ling, R. Luo, H. Liang, M. Li, B. Shen, H. Wang, K. Vahala, and Q. Lin, "Self-starting bi-chromatic $LiNbO_3$ soliton microcomb," Optica **6**, 1138 (2019).
9. S. Wan, R. Niu, J.-L. Peng, J. Li, G.-C. Guo, C.-L. Zou, and C.-H. Dong, "Fabrication of the high-Q Si_3N_4 microresonators for soliton microcombs," Chin. Opt. Lett. **20**, 032201 (2022).
10. Ó. B. Helgason, M. Girardi, Z. Ye, F. Lei, J. Schröder, and V. T. Company, "Power-efficient soliton microcombs," arXiv:2202.09410 (2022).
11. X. Xue, X. Zheng, and B. Zhou, "Super-efficient temporal solitons in mutually coupled optical cavities," Nat. Photonics **13**, 616 (2019).
12. X. X. Xue, Y. Xuan, Y. Liu, P.-H. Wang, S. Chen, J. Wang, D. E. Leaird, M. Qi, and A. M. Weiner, "Mode-locked dark pulse Kerr combs in normal-dispersion microresonators," Nat. Photonics **9**, 594 (2015).
13. D. C. Cole, E. S. Lamb, P. Del'Haye, S. A. Diddams, and S. B. Papp, "Soliton crystals in Kerr resonators," Nat. Photonics **11**, 671 (2017).
14. E. Obrzud, S. Lecomte, and T. Herr, "Temporal solitons in microresonators driven by optical pulses," Nat. Photonics **11**, 600 (2017).
15. T. Liu, S. Sun, Y. Gao, S. Wang, Y. Chu, and H. Guo, "Optical microcombs in whispering gallery mode crystalline resonators with broadband intermode interactions," arXiv:2203.13973 (2022).
16. Y. Bai, M. Zhang, Q. Shi, S. Ding, Y. Qin, Z. Xie, X. Jiang, and M. Xiao, "Brillouin–Kerr soliton frequency combs in an optical microresonator," Phy. Rev. Lett. **126**, 063901 (2021).
17. H. Guo, M. Karpov, E. Lucas, A. Kordts, M. H. P. Pfeiffer, V. Brasch, G. Lihachev, V. E. Lobanov, M. L. Gorodetsky, and T. J. Kippenberg, "Universal dynamics and deterministic switching of dissipative Kerr solitons in optical microresonators," Nat. Photonics **13**, 94 (2017).
18. X. Liu, Z. Gong, A. W. Bruch, J. B. Surya, J. Lu, and H. X. Tang, "Aluminum nitride nanophotonics for beyond-octave soliton microcomb generation and self-referencing," Nat. Commun. **12**, 5428 (2021).
19. C. Bao, L. Zhang, A. Matsko, Y. Yan, Z. Zhao, G. Xie, A. M. Agarwal, L. C. Kimerling, J. Michel, L. Maleki, and A. E. Willner, "Nonlinear conversion efficiency in Kerr frequency comb generation," Opt. Lett. **39**, 6126 (2014).
20. S. Coen, H. G. Randle, T. Sylvestre, and M. Erkintalo, "Modeling of octave-spanning Kerr frequency combs using a generalized mean-field Lugiato–Lefever model," Opt. Lett. **38**, 37 (2013).
21. S. B. Papp, P. Del'Haye, and S. A. Diddams, "Mechanical control of a microrod-resonator optical frequency comb," Phys. Rev. X **3**, 031003 (2013).
22. X. Yi, Q.-F. Yang, K. Y. Yang, M.-G. Suh, and K. Vahala, "Soliton frequency comb at microwave rates in a high-Q silica microresonator," Optica **2**, 1078 (2015).
23. L. Yao, P. Liu, H.-J. Chen, Q. H. Gong, Q.-F. Yang, and Y.-F. Xiao, "Soliton microwave oscillators using oversized billion Q optical microresonators," Optica **9**, 561 (2022).
24. M.-G. Suh and K. Vahala, "Gigahertz-repetition-rate soliton microcombs," Optica **5**, 65 (2018).
25. T. J. Kippenberg, S. M. Spillane, and K. J. Vahala, "Kerr-nonlinearity optical parametric oscillation in an ultrahigh-Q toroid microcavity," Phys. Rev. Lett. **93**, 083904 (2004).
26. X. Ji, F. A. S. Barbosa, S. P. Roberts, A. Dutt, J. Cardenas, Y. Okawachi, A. Bryant, A. L. Gaeta, and M. Lipson, "Ultra-low-loss on-chip resonators with sub-milliwatt parametric oscillation threshold," Optica **4**, 619 (2017).
27. L. Chang, W. Xie, H. Shu, Q.-F. Yang, B. Shen, A. Boes, J. D. Peters, W. Jin, C. Xiang, S. Liu, G. Moille, S.-P. Yu, X. Wang, K. Srinivasan, S. B. Papp, K. Vahala, and J. E. Bowers, "Ultra-efficient frequency comb generation in AlGaAs-on-insulator microresonators," Nat. Commun. **11**, 1331 (2020).
28. L. Razzari, D. Duchesne, M. Ferrera, R. Morandotti, S. Chu, B. E. Little, and D. J. Moss, "CMOS-compatible integrated optical hyper-parametric oscillator," Nat. Photonics **4**, 41 (2010).
29. A. G. Griffith, R. K. W. Lau, J. Cardenas, Y. Okawachi, A. Mohanty, R. Fain, Y. H. D. Lee, M. Yu, C. T. Phare, C. B. Poitras, A. L. Gaeta, and M. Lipson, "Silicon-chip mid-infrared frequency comb generation," Nat. Commun. **6**, 6299 (2015).
30. D. J. Wilson, S. Hönl, K. Schneider, M. Anderson, T. J. Kippenberg, and P. Seidler, "Gallium phosphide microresonator frequency combs," in *Conference on Lasers and Electro-Optics (CLEO)* (2018), paper JW3I.5.
31. Z. Gong, A. Bruch, M. Shen, X. Guo, H. Jung, L. Fan, X. Liu, L. Zhang, J. Wang, J. Li, J. Yan, and H. X. Tang, "High-fidelity cavity soliton generation in crystalline AlN micro-ring resonators," Opt. Lett. **43**, 4366 (2018).
32. Q. Wen, J. Qin, Y. Geng, K. Qiu, and H. Zhou, "Fabrication and excitation of single whispering gallery mode microdisk resonator," in *Asia Communications and Photonics Conference (ACP)* (2019), paper M4A.233.